International Journal of Solids and Structures 67–68 (2015) 93–101

Contents lists available at ScienceDirect

International Journal of Solids and Structures

journal homepage: www.elsevier.com/locate/ijsolstr

# Modeling of deformation and localized failure in anisotropic rocks

S. Pietruszczak *, E. Haghighat

*Department of Civil Engineering, McMaster University, Hamilton, ON, Canada*

ARTICLE INFO

*Article history:*
Received 8 November 2014
Received in revised form 26 March 2015
Available online 9 April 2015

*Keywords:*
Constitutive modeling
Anisotropy
Localization
Discrete crack propagation
Embedded discontinuity

ABSTRACT

This paper deals with description of the deformation process in argillaceous rocks that display a strong inherent anisotropy. Both, the homogeneous and the localized deformation modes are considered. The effects of anisotropy are incorporated by invoking the microstructure tensor approach. The strain localization is assumed to be associated with formation of a macrocrack the orientation of which is defined using the critical plane approach. The propagation of damage is traced within the context of a boundary value problem by employing a constitutive law with embedded discontinuity. The crack path is monitored in a discrete manner by using the level-set method. The closest-point projection algorithm is developed for the integration of the constitutive relations at both stages of the anisotropic deformation process, i.e. the homogenous mode as well as that involving an embedded discontinuity. The problem of macrocrack formation in a biaxial plane strain compression test is studied. It is demonstrated that friction between loading platens can play an important role in the process of evolution of damage and may significantly affect the compressive strength.



## 1. Introduction

Many geomaterials display a structural anisotropy which is closely related to their microstructure. The primary focus here is on the sedimentary rocks formed by compaction, cementation or crystallization of successive layers of deposited material. These rocks, which include shale and slate, are characterized by the presence of closely spaced bedding planes and exhibit a strong directional dependence of strength as well as deformation properties. The understanding of the mechanical behaviour of argillaceous rocks is of a significant importance due to their widespread applications in many types of geotechnical projects, including petroleum extraction, carbon dioxide sequestration as well as a deep geological disposal of radioactive waste. The primary concern in this case is the onset and propagation of damage due to excavation, transport of pore fluids and/or the elevated temperature.

The description of the mechanical behaviour requires, first of all, the specification of conditions at failure under an arbitrary stress state. In addition, a general framework must be provided for the evaluation of the deformation field, which may include discontinuities such as macrocracks. Over the last few decades, an extensive research effort has been devoted to modeling of the mechanical behaviour of anisotropic rocks. A comprehensive review on this topic, examining different approaches, is provided in the articles by Duveau and Henry (1998) and Kwasniewski (1993). One of the first attempts to describe the conditions at failure in anisotropic rocks was the work reported by Pariseau (1968), which was an extension of Hill's criterion (Hill, 1950). This was followed by more complex tensorial representations (Amadei, 1983; Boehler and Sawczuk, 1977; Nova, 1980). The application of the latter criteria to practical problems is generally difficult due to a large number of independent material functions/parameters that appear in the formulation. A simple and pragmatic approach, which incorporates a scalar anisotropy parameter that is a function of a mixed invariant of the stress and the structure orientation tensor, has been developed by Pietruszczak and Mroz (2001). This approach was later applied to modeling of sedimentary rocks (Lade, 2007; Pietruszczak et al., 2002).

Numerical approaches dealing with crack propagation in continuous isotropic media have been investigated for several decades. Many attempts have been made to accurately model both the smeared nature of the onset of cracking at initial stages of loading as well as the discrete nature of macrocrack propagation. The research started in early 1960s when the node separation technique was introduced (Ngo and Scordelis, 1967). This was followed by the adaptive remeshing (Ingraffea, 1977) as well as introduction of the smeared damage models (Bažant and Cedolin, 1979; Nayak and Zienkiewicz, 1972; Rashid, 1968). The issue of mesh-size dependency was first addressed in the early 1980s within the context of a constitutive law with embedded discontinuity (Pietruszczak and Mroz, 1981; see also Pietruszczak, 1999). Later, several attempts

* Corresponding author. Tel.: +1 (905) 925 9140x24007.
*E-mail address:* pietrusz@mcmaster.ca (S. Pietruszczak).

http://dx.doi.org/10.1016/j.ijsolstr.2015.04.004
0020-7683/

were made to incorporate the discontinuous motion into the interpolation functions (Belytschko et al., 1994; Fish and Belytschko, 1988; Simo et al., 1993). The concept of reproducing kernels (Liu et al., 1995) and partition of unity (Melenk and Babuška, 1996) resulted in development of a methodology for modeling crack propagation through the Extended Finite Element Method X-FEM (Belytschko and Black, 1999; Moës et al., 1999; Sukumar et al., 2000). This approach was then combined with the level-set method for tracing of the paths crack propagation (Chessa and Belytschko, 2003) and was applied to a broad class of problems providing stable, mesh independent results. The only concern in relation to this approach is the necessity of dealing with additional enrichment functions for the cracked elements. The latter requires updating mesh data structures throughout the analysis as well as the use of a special integration technique. In a recent study, the idea of tracing the propagating crack in a discrete way was combined with the embedded discontinuity approach (Haghighat and Pietruszczak, 2015) and applied to modeling of crack/shear band inception and propagation. The approach shows an accurate mesh-independent response without requiring any special techniques in terms of implementation.

This paper is an extension of the work reported earlier (Pietruszczak et al., 2002) and deals with description of the deformation process in argillaceous rocks. Both, the homogeneous and the localized modes are considered here while the effects of anisotropy are incorporated by invoking the microstructure tensor approach. The strain localization is assumed to be associated with formation of a macrocrack and a simple methodology is proposed for identifying the orientation of the crack based on the critical plane approach. In section two, the plasticity framework incorporating an anisotropic deviatoric hardening model is presented, followed by the formulation of a constitutive model with embedded discontinuity. The section is concluded by introducing a simple criterion for initiation of crack and specification of its orientation. In section three, the closest-point projection algorithm is developed for the integration of the constitutive relations at both stages of the anisotropic deformation process. Section four focuses on numerical modeling of shear band formation in biaxial tests conducted on Tournemire argillite. The crack path is monitored in a discrete manner by using the level-set method. The effects of boundary conditions, orientation of bedding planes, and mesh-sensitivity of the approach are studied. It is demonstrated that friction between loading platens can play an important role in the process of evolution of damage and may significantly affect the strength characteristics that are commonly perceived as a material property.

## 2. Formulation of the problem

The deformation process in argillaceous rocks incorporates two main stages; the first one is associated with a homogeneous deformation and the second one involves a failure mode associated with inception of a macrocrack. Thus, in order to describe the mechanical behaviour, one has to formulate a constitutive relation dealing with an inherently anisotropic response prior to failure, an appropriate failure criterion, and a framework describing the post-failure response involving the localized deformation. These three key points are addressed below. First, an anisotropic *deviatoric hardening* model is presented describing the response prior to the onset of failure. Then, a failure criterion is introduced which incorporates the critical plane approach for identifying the direction of the macrocrack. Finally, a constitutive law with embedded discontinuity is introduced that is capable of describing the post localization response within a selected reference volume. In the last case, the dominant factor controlling the mechanical characteristics is the interfacial response.

### 2.1. Constitutive relation describing the homogeneous deformation mode

The elasto-plastic framework employed in this study incorporates the microstructure tensor approach (Pietruszczak and Mroz, 2001). In order to define the anisotropy parameter(s), the formulation employs a generalized *loading vector* that is defined as

$$\boldsymbol{L} = L_\alpha \boldsymbol{e}^{(\alpha)}; \quad L_\alpha^2 = \mathbf{t}^{(\alpha)} \cdot \mathbf{t}^{(\alpha)} = (\boldsymbol{e}^{(\alpha)} \cdot \boldsymbol{\sigma}) \cdot (\boldsymbol{e}^{(\alpha)} \cdot \boldsymbol{\sigma}) \tag{1}$$

where $\boldsymbol{e}^{(\alpha)}, \alpha = 1,2,3$, are the unit vectors, which specify the preferred material axes. Thus, the components of $\boldsymbol{L}$ represent the magnitudes of tractions on planes normal to the principal material axes. Introduce now a microstructure tensor $\boldsymbol{a}$, which is a measure of material fabric. While different descriptors may be employed to quantify the fabric, the eigenvectors of this operator define the orientation of the base vectors $\boldsymbol{e}^{(\alpha)}$. The projection of the microstructure tensor on the direction $\boldsymbol{L}$ becomes

$$\vartheta = \boldsymbol{\ell} \cdot \boldsymbol{a} \cdot \boldsymbol{\ell}; \quad \boldsymbol{\ell} = \boldsymbol{L}/(\boldsymbol{L} \cdot \boldsymbol{L})^{1/2} \tag{2}$$

Here, the scalar variable $\vartheta$, referred to as anisotropy parameter, specifies the effect of load orientation relative to material axes and can be defined as the ratio of joint invariant of stress and microstructure tensor $tr(\boldsymbol{\sigma} \cdot \boldsymbol{a} \cdot \boldsymbol{\sigma})$ to the second invariant of the stress tensor (cf. Pietruszczak and Mroz (2001)). It is a homogeneous function of stress of the degree zero, so that the stress magnitude does not affect its value. Note that Eq. (2) can be expressed as

$$\vartheta = \vartheta_0(1 + \boldsymbol{\ell} \cdot \boldsymbol{A} \cdot \boldsymbol{\ell}) = \vartheta_0(1 + \zeta); \quad \zeta = \boldsymbol{\ell} \cdot \boldsymbol{A} \cdot \boldsymbol{\ell} \tag{3}$$

where $\boldsymbol{A} = dev(\boldsymbol{a})/\vartheta_0$ is a symmetric traceless tensor and $\vartheta_0 = tr(\boldsymbol{a})/3$. The representation (3) can be generalized by employing a polynomial expansion which incorporates higher order terms in dyadic products $\zeta$, i.e.

$$\vartheta = \vartheta_0 (1 + \zeta + a_1\zeta^2 + a_2\zeta^3 + a_3\zeta^4 + \cdots) \tag{4}$$

where $a_1, a_2, a_3, \ldots$ are the expansion coefficients. Using the notion of this scalar anisotropy parameter, as defined viz. Eq. (4), any isotropic failure criterion can be extended to the case of anisotropy by assuming

$$F(\boldsymbol{\sigma}) = F(I_1, I_2, I_3, \zeta) \tag{5}$$

where $I_1, I_2, I_3$ are the basic stress invariants. It should be noted that for materials with strong inherent anisotropy, as discussed here, the representation (5) does not require a specific fabric descriptor. This is because the principal material directions are known *a priori* and do not change. An explicit definition is required only in the context of evolving (i.e. induced) anisotropy.

The parameter $\zeta$ is typically identified with the strength descriptor(s), which is embedded in the failure function $F$; its value is then assumed to depend on the orientation of the sample relative to the direction of loading. In this work a simple linear form of Eq. (5) has been adopted, which corresponds to the well-known Mohr–Coulomb criterion, i.e.

$$F(\boldsymbol{\sigma}) \equiv F(\sigma_m, \bar{\sigma}, \theta, \zeta) = \sqrt{3}\bar{\sigma} - \eta_f(\zeta) g(\theta)(\sigma_m + C) = 0 \tag{6}$$

Here, $\sigma_m = -tr(\boldsymbol{\sigma})/3$, $\bar{\sigma} = \sqrt{tr(\mathbf{s} \cdot \mathbf{s})/2}$, where $\mathbf{s}$ is the deviatoric part of stress tensor; while $\theta$, which is defined as $\theta = -\sin^{-1}(\sqrt{27/4}J_3/\bar{\sigma}^3)/3$ with $J_3 = tr(\mathbf{s} \cdot \mathbf{s} \cdot \mathbf{s})/3$, denotes the Lode's angle. Moreover,

$$g(\theta) = \frac{3 - \sin\phi}{2\sqrt{3}\cos\theta - 2\sin\theta\sin\phi}; \quad \eta_f = \frac{6\sin\phi}{3 - \sin\phi}; \quad C = c\cot\phi \tag{7}$$

where $\phi, c$ are the angle of friction and cohesion, respectively. Note that the strength descriptors, in this case $\eta_f$ and $C$, are assumed to be orientation-dependent and have the representation analogous to

that of Eq. (4). However, in the context of the failure criterion (6), the parameter $C$ is associated with a hydrostatic stress state. The latter is, in fact, invariant with respect to orientation of the sample. Thus, the effects of anisotropy can be primarily attributed to variation in the strength parameter $\eta_f$.

The general plasticity formulation can be derived by assuming the yield/loading surface in the form consistent with representation (6), i.e.

$$f = \sqrt{3}\bar{\sigma} - \eta g(\theta)(\sigma_m + C) = 0; \quad \eta = \eta(\kappa,\zeta) = \eta_f(\zeta)\frac{\xi\kappa}{A+\kappa};$$
$$d\kappa = \left(\frac{2}{3}\dot{\boldsymbol{e}}^p : \dot{\boldsymbol{e}}^p\right)^{1/2} \tag{8}$$

where $\dot{\boldsymbol{e}}^p$ is the deviatoric part of the plastic strain rate and $A$ and $\xi$ are material parameters. According to the hardening rule, for $\kappa \to \infty$ there is $\eta \to \xi\eta_f$, where $\xi > 1$. The parameter $\xi$ is introduced here in order to define the transition to localized deformation, which is assumed to occur at $\eta = \eta_f$. Note that the latter equality implies that $f = F$, so that the conditions at failure are consistent with Mohr–Coulomb criterion (6). The plastic potential can be chosen as

$$\psi = \sqrt{3}\bar{\sigma} + \eta_c g(\theta)(\sigma_m + C)\ln\frac{(\sigma_m + C)}{\sigma_m^0} = 0 \tag{9}$$

where, $\eta_c$ is the dilatancy coefficient defined as $\eta_c = \alpha\eta_f$ with $\alpha$ assumed as a material constant. It should be mentioned that the choice of this function is motivated by its ability to describe a progressive transition from compaction to dilatancy, which is typical for sedimentary rocks (Pietruszczak et al., 2002).

Now, the constitutive relation can be expressed in the general form

$$\boldsymbol{\sigma} = \mathbb{D} : \dot{\boldsymbol{\varepsilon}}^e = \mathbb{D} : (\dot{\boldsymbol{\varepsilon}} - \dot{\boldsymbol{\varepsilon}}^p), \quad \dot{\boldsymbol{\varepsilon}}^p = \dot{\lambda}\partial_{\boldsymbol{\sigma}}\psi \tag{10}$$

where the yield and potential functions are defined by Eqs. (8) and (9). Here, $\mathbb{D}$ is the anisotropic elastic operator. For an elastic loading trajectory, $\dot{\lambda} = 0$, which implies $\dot{\boldsymbol{\varepsilon}}^p = 0$. For an active (plastic) loading process, $f(\boldsymbol{\sigma}, \kappa) = 0$ and $\dot{\lambda} > 0$. Imposing the consistency condition, the plastic multiplier can be expressed as

$$\partial_{\boldsymbol{\sigma}} f : \dot{\boldsymbol{\sigma}} + \partial_\lambda f\,\dot{\lambda} = 0 \to \dot{\lambda} = \frac{\partial_{\boldsymbol{\sigma}} f : \mathbb{D} : \dot{\boldsymbol{\varepsilon}}^e}{\partial_{\boldsymbol{\sigma}} f : \mathbb{D} : \partial_{\boldsymbol{\sigma}}\psi - \partial_\lambda f} \tag{11}$$

where

$$\partial_{\boldsymbol{\sigma}} f = \frac{\partial f}{\partial\sigma_m}\partial_{\boldsymbol{\sigma}}\sigma_m + \frac{\partial f}{\partial\bar{\sigma}}\partial_{\boldsymbol{\sigma}}\bar{\sigma} + \frac{\partial f}{\partial\theta}\partial_{\boldsymbol{\sigma}}\theta + \frac{\partial f}{\partial\zeta}\partial_{\boldsymbol{\sigma}}\zeta$$
$$\partial_{\boldsymbol{\sigma}}\psi = \frac{\partial\psi}{\partial\sigma_m}\partial_{\boldsymbol{\sigma}}\sigma_m + \frac{\partial\psi}{\partial\bar{\sigma}}\partial_{\boldsymbol{\sigma}}\bar{\sigma} + \frac{\partial\psi}{\partial\theta}\partial_{\boldsymbol{\sigma}}\theta + \frac{\partial\psi}{\partial\zeta}\partial_{\boldsymbol{\sigma}}\zeta \tag{12}$$

Substituting Eq. (11) back into Eq. (10), the tangential elasto-plastic operator $\mathbb{D}_T$ can be defined as

$$\boldsymbol{\sigma} = \mathbb{D}_T : \dot{\boldsymbol{\varepsilon}}, \quad , \mathbb{D}_T = \mathbb{D} - \frac{(\mathbb{D} : \partial_{\boldsymbol{\sigma}}\psi) \otimes (\partial_{\boldsymbol{\sigma}} f : \mathbb{D})}{\partial_{\boldsymbol{\sigma}} f : \mathbb{D} : \partial_{\boldsymbol{\sigma}}\psi - \partial_\lambda f} \tag{13}$$

The integration scheme for the above constitutive relation is presented in Section 3.

### 2.2. Description of localized deformation: a constitutive law with embedded discontinuity (CLED)

A discontinuous motion within a body can be expressed in the form

$$\mathbf{v}(\mathbf{x},t) = \hat{\mathbf{v}}(\mathbf{x},t) + \mathcal{H}(\phi)\tilde{\boldsymbol{v}}(\mathbf{x},t) \tag{14}$$

where $\hat{\mathbf{v}}$ and $\tilde{\boldsymbol{v}}$ are two continuous functions and $\mathcal{H}(\phi)$ is the Heaviside step function. The latter depends on $\phi = \phi(\mathbf{x}, t)$, which is the level-set function that represents the geometry of the crack. The symmetric part of the gradient operator of (14) can be expressed as

$$\nabla^s\mathbf{v}(\mathbf{x},t) = \nabla^s\hat{\mathbf{v}}(\mathbf{x},t) + \mathcal{H}(\phi)\nabla^s\tilde{\mathbf{v}}(\mathbf{x},t) + \delta(\phi)(\mathbf{n}\otimes\tilde{\mathbf{v}})^s \tag{15}$$

Note that $\nabla^s\mathcal{H}(\phi) = \delta(\phi)\nabla\phi$, where $\delta$ is the Dirac delta function defined as being singular at $\phi = 0$ and zero elsewhere. The gradient of a level-set function represents the normal to the surface, i.e. $\nabla\phi = \mathbf{n}$. The level-set that is employed here is the signed distance function, i.e. $\phi(\mathbf{x}) = \text{sign}\{\mathbf{n}_\Gamma\cdot(\mathbf{x}-\mathbf{x}_\Gamma)\}\min\|\mathbf{x}-\mathbf{x}_\Gamma\|$, as introduced in Sukumar et al. (2001). As mentioned in the introduction, different methodologies can be used to incorporate the discontinuous motion into the solution. In the approach pursued here the discontinuity is embedded in the constitutive law by averaging the localized deformation over the considered reference volume.

Examining Eq. (15), it can be noted that the first two terms describe the motion in the intact part of the reference volume while the third term that involves the Dirac function is associated with the localized deformation along the crack. Taking the volume average of the last term, one has

$$\frac{1}{\Delta v}\int_{\Delta v}\delta(\phi)(\mathbf{n}\otimes\dot{\mathbf{g}})^s d\Omega = \frac{1}{\Delta v}\int_{\Delta a}(\mathbf{n}\otimes\dot{\mathbf{g}})^s d\Gamma \tag{16}$$

Here, $\Delta a$ represents the surface area of the crack within the considered volume $\Delta v$, while $\dot{\mathbf{g}}$ is the discontinuous motion along the interface, i.e. $\dot{\mathbf{g}} = [\![\mathbf{v}]\!] = [\![\mathcal{H}]\!]\tilde{\mathbf{v}}$. Ignoring the variation of this discontinuous motion within a small enough $\Delta v$, one may express Eq. (16) as

$$\frac{1}{\Delta v}\int_{\Delta v}\delta(\phi)(\mathbf{n}\otimes\dot{\mathbf{g}})^s d\Omega \approx \chi(\mathbf{n}\otimes\dot{\mathbf{g}})^s \quad \text{with} \quad \chi = \frac{\Delta a}{\Delta v} \tag{17}$$

Thus, the total strain rate can be divided into two elementary parts. The first one, denoted as $\dot{\bar{\boldsymbol{\varepsilon}}}$, is associated with the intact part of the reference volume, while the other one, referred to as $\dot{\tilde{\boldsymbol{\varepsilon}}}$, represents the discontinuous motion along the crack averaged over this volume, i.e.

$$\dot{\boldsymbol{\varepsilon}} = \dot{\bar{\boldsymbol{\varepsilon}}} + \dot{\tilde{\boldsymbol{\varepsilon}}} \quad \text{where} \quad \dot{\tilde{\boldsymbol{\varepsilon}}} = \chi(\mathbf{n}\otimes\dot{\mathbf{g}})^s \tag{18}$$

Adopting the additivity of strain rates, the stress field can be defined as

$$\dot{\boldsymbol{\sigma}} = \mathbb{D} : \dot{\bar{\boldsymbol{\varepsilon}}} = \mathbb{D} : (\dot{\boldsymbol{\varepsilon}} - \dot{\tilde{\boldsymbol{\varepsilon}}}) \tag{19}$$

In order to determine the velocity discontinuity $\dot{\mathbf{g}}$ that is embedded in the constitutive relation (19), the continuity of the rate of traction along the interface is imposed, i.e. $\dot{\mathbf{t}} = \mathbf{n}\cdot\dot{\boldsymbol{\sigma}}$. Thus,

$$\{\mathbf{n}\cdot\dot{\boldsymbol{\sigma}} = \mathbf{n}\cdot\mathbb{D}\cdot\dot{\boldsymbol{\varepsilon}} - \chi\mathbf{n}\cdot\mathbb{D}\cdot(\mathbf{n}\otimes\dot{\mathbf{g}})\} = \{\dot{\mathbf{t}} = \mathbf{K}\cdot\dot{\mathbf{g}}\}$$
$$\to \dot{\tilde{\boldsymbol{\varepsilon}}} = \mathbb{E} : \mathbb{D} : \dot{\boldsymbol{\varepsilon}}; \quad \mathbb{E} = \chi\mathbf{n}\otimes(\mathbf{K} + \chi\mathbf{n}\cdot\mathbb{D}\cdot\mathbf{n})^{-1}\otimes\mathbf{n} \tag{20}$$

where $\mathbf{K}$ is the tangential operator which defines the interfacial properties. Thus, the constitutive relation within the region experiencing the discontinuous motion may be finally expressed as

$$\dot{\boldsymbol{\sigma}} = \tilde{\mathbb{D}} : \dot{\boldsymbol{\varepsilon}} \quad \text{where} \quad \tilde{\mathbb{D}} = \mathbb{D} - \mathbb{D} : \mathbb{E} : \mathbb{D} \tag{21}$$

where $\tilde{\mathbb{D}}$ is the tangential operator. The integration scheme for the above constitutive relation is derived in Section 3. Further details regarding the implementation and the procedure for tracing the crack are provided in Haghighat and Pietruszczak (2015).

### 2.3. Specification of the orientation of macrocrack at its inception

The issue of the onset of localization may be perceived as a bifurcation problem (Rudnicki and Rice, 1975). Such an approach, although mathematically rigorous, strongly relies on the constitutive description of homogeneous deformation, including the type of hardening and/or flow rule, and the predictions are not always

consistent with the experimental evidence. A simpler approach is to assume that the inception of localized damage occurs when the failure function reaches a critical value. For the analysis conducted in this work, the Mohr–Coulomb criterion (6) is checked at every Gauss point within the volume of a finite element that is considered as the reference volume. If the average value of $F$ approaches zero, the element is said to undergo a discontinuous motion; the level-set is updated and the next load increment is applied. In order to carry out the integration of the constitutive law (21), the orientation of the macrocrack must be defined. This is accomplished by invoking the critical plane approach as explained below.

Within the context of the critical plane framework (Pietruszczak and Mroz, 2001), the failure function is defined as a function of the components of traction vector $\mathbf{t} = \mathbf{n} \cdot \boldsymbol{\sigma}$ acting on a plane with unit normal $\mathbf{n}$. For reproducing the bias in the special distribution of strength parameters, say $h(\mathbf{n})$, a scalar descriptor $\varphi$ is defined such that

$$F = F[\mathbf{t}, h(\mathbf{n})];$$
$$h = \hat{h}(1 + \varphi + b_1\varphi^2 + b_2\varphi^3 + b_3\varphi^4 + \cdots), \quad \varphi = \mathbf{n} \cdot \boldsymbol{\Omega} \cdot \mathbf{n} \tag{22}$$

where, $b_1, b_2, b_3$ are constants and $\boldsymbol{\Omega}$ is a symmetric traceless tensor whose eigenvectors coincide with the principle material axis.

Thus, the Coulomb failure function can be expressed here as

$$F = |\tau| - (\mu_f \sigma + c) \tag{23}$$

where $\tau$, $\sigma$ are tangential and normal components of traction $\mathbf{t}$, and the friction coefficient $\mu_f$ as well as cohesion $c$ are both assumed to be orientation dependent, i.e. $\mu_f = \mu_f(\mathbf{n})$ and $c = c(\mathbf{n})$, and their distribution is defined viz. representation (22). The problem of the specification of the direction of macrocrack can then be defined as a constrained optimization problem for failure function (22), i.e.

$$\max_{\mathbf{n}} F = \max_{\mathbf{n}} F[\mathbf{t}, h(\mathbf{n})] \mid F = 0 \wedge \mathbf{n} \cdot \mathbf{n} = 1 \tag{24}$$

The above equation may be solved by any known optimization technique, such as Lagrange multipliers, and the result would define the direction of the localization plane at any integration point.

It should be noted that the conditions at failure as stipulated by Eqs. (23) and (24) are consistent with the Mohr–Coulomb representation (6) provided the strength parameters $h(\mathbf{n})$, Eq. (22), are properly identified. This issue is addressed further in Section 4, which deals with the numerical implementation. In general, the solution will provide two conjugate orientations. Here, the orientation that maximizes the product $\Delta\boldsymbol{\varepsilon} : (\mathbf{n} \otimes \mathbf{m})$, where $\mathbf{m}$ is the direction of discontinuous motion $\mathbf{g}$, is selected to define the prevailing orientation of the localization plane, as suggested by Rabczuk and Belytschko (2007).

## 3. The numerical integration schemes

As indicated in the previous section, the deformation process involves two stages; one deals with a homogeneous deformation that is governed by the constitutive law (13) and the other one is associated with localized deformation, viz. Eq. (21). In what follows, the implicit integration schemes for both these cases are derived.

### 3.1. The integration scheme for elasto-plastic model governing the homogeneous deformation mode

In this case, in order to simplify the algebra, it is convenient to refer the problem to the coordinate system associated with the principal material axes. According to Eq. (10), the constitutive relation takes the form

$$\boldsymbol{\sigma} = \boldsymbol{\sigma}_t + \mathbb{D} : (\Delta\boldsymbol{\varepsilon} - \Delta\boldsymbol{\varepsilon}^p), \quad \Delta\boldsymbol{\varepsilon}^p = \Delta\lambda\partial_{\boldsymbol{\sigma}}\psi \tag{25}$$

where $\mathbb{D}$ is the elastic stiffness operator, $\psi$ is the potential function defined in Eq. (9) and $\Delta\lambda$ is the plastic multiplier. Here, the variables without a subscript refer to time $t + \Delta t$. Using the closest point projection approach (Simo, 1998), the plastic strain and the yield function residuals at time $t + \Delta t$ can be expressed as

$$\mathbf{R}^{(k)} \equiv -\boldsymbol{\varepsilon}^{p(k)} + \boldsymbol{\varepsilon}_n^p + \Delta\lambda^{(k)}\partial_{\boldsymbol{\sigma}}\psi^{(k)}$$
$$f^{(k)} \equiv f(\boldsymbol{\sigma}^{(k)}, \kappa^{(k)}) \tag{26}$$

Linearizing the above equations, one can write

$$\mathbf{R}^{(k)} + \partial_{\boldsymbol{\sigma}}\mathbf{R}^{(k)} : \delta\boldsymbol{\sigma}^{(k)} + \partial_\lambda\mathbf{R}^{(k)}\delta\lambda^{(k)} = 0$$
$$f^{(k)} + \partial_{\boldsymbol{\sigma}}f^{(k)} : \delta\boldsymbol{\sigma}^{(k)} + \partial_\lambda f^{(k)}\delta\lambda^{(k)} = 0 \tag{27}$$

with the derivatives expressed as $\partial_{\boldsymbol{\sigma}}\mathbf{R}^{(k)} = \mathbb{C} + \Delta\lambda\,\partial^2_{\boldsymbol{\sigma}}\psi$ and $\partial_\lambda\mathbf{R}^{(k)} = \partial_{\boldsymbol{\sigma}}\psi$, where $\mathbb{C}$ is the compliance operator. Denoting $\mathbb{Q} = \partial_{\boldsymbol{\sigma}}\mathbf{R}^{-1}$, the plastic multiplier, stress and plastic strain corrections can be determined as

$$\delta\lambda^{(k)} = \frac{f^{(k)} - \partial_{\boldsymbol{\sigma}}f^{(k)} : \mathbb{Q}^{(k)} : \mathbf{R}^{(k)}}{\partial_{\boldsymbol{\sigma}}f^{(k)} : \mathbb{Q}^{(k)} : \partial_{\boldsymbol{\sigma}}\psi^{(k)} - \partial_\lambda f^{(k)}}$$
$$\delta\boldsymbol{\sigma}^{(k)} = -\mathbb{Q}^{(k)} : \left[\mathbf{R}^{(k)} + \partial_{\boldsymbol{\sigma}}\psi^{(k)}\delta\lambda^{(k)}\right] \tag{28}$$
$$\delta\boldsymbol{\varepsilon}^{p\,(k)} = -\mathbb{C} : \delta\boldsymbol{\sigma}^{(k)}$$

and the updated variables can be specified as

$$\Delta\lambda^{(k+1)} = \Delta\lambda^{(k)} + \delta\lambda^{(k)}$$
$$\boldsymbol{\sigma}^{(k+1)} = \boldsymbol{\sigma}^{(k)} + \delta\boldsymbol{\sigma}^{(k)} \tag{29}$$
$$\boldsymbol{\varepsilon}^{p(k+1)} = \boldsymbol{\varepsilon}^{p(k)} + \delta\boldsymbol{\varepsilon}^{p(k)}$$

Note that the anisotropy parameter $\vartheta$ is embedded in the gradient operators $\partial_{\boldsymbol{\sigma}}f, \partial_{\boldsymbol{\sigma}}\psi$ as indicated in Eq. (12)

### 3.2. The integration scheme for constitutive model with embedded discontinuity

Considering Eq. (19), one can express the stress state in the intact material at $t + \Delta t$ as

$$\boldsymbol{\sigma} = \boldsymbol{\sigma}_t + \mathbb{D} : (\Delta\boldsymbol{\varepsilon} - \Delta\tilde{\boldsymbol{\varepsilon}}) \quad \text{where} \quad \Delta\tilde{\boldsymbol{\varepsilon}} = \chi(\mathbf{n} \otimes \Delta\mathbf{g})^s \tag{30}$$

The interfacial constitutive model can be defined as

$$\mathbf{t} = \mathbf{t}_t + \mathbf{K} \cdot (\Delta\mathbf{g} - \Delta\mathbf{g}^p), \quad \Delta\mathbf{g}^p = \Delta\gamma\partial_{\mathbf{t}}\psi \tag{31}$$

In the examples provided in Section 4, the yield and plastic potential functions for the interface material are taken in a simple linear form

$$\mathrm{f} \equiv \mathrm{f}(\mathbf{t}, g) = |\tau| + \mu_f(g)\sigma = 0, \quad \psi \equiv \psi(\mathbf{t}) = |\tau|$$
$$\mu_f = \mu_f^r + (\mu_f^0 - \mu_f^r)\exp(-\omega g) \tag{32}$$

where $g$ is the tangential component of plastic part of velocity discontinuity and $\mu_f$ is the friction coefficient. The latter is assumed to be monotonically decreasing according to an exponential relation (32), in which $\mu_f^0, \mu_f^r$ are the initial and residual values of $\mu_f$ and the rate of degradation is governed by the parameter $\omega$.

Imposing the consistency condition $\Delta\mathrm{f} = 0$ along the interface, one obtains

$$\Delta\mathbf{t} = \mathbf{K}^{ep} \cdot \Delta\mathbf{g} \quad \text{where} \quad \mathbf{K}^{ep} = \mathbf{K} - \frac{(\mathbf{K} \cdot \partial_{\mathbf{t}}\psi) \otimes (\partial_{\mathbf{t}}\mathrm{f} \cdot \mathbf{K})}{\partial_{\mathbf{t}}\mathrm{f} \cdot \mathbf{K} \cdot \partial_{\mathbf{t}}\psi - \partial_g\mathrm{f}} \tag{33}$$

In order to formulate the return mapping scheme, the following residuals are introduced

$$\mathbf{R}_1^{(k)} \equiv -\tilde{\boldsymbol{\varepsilon}}^{(k)} + \tilde{\boldsymbol{\varepsilon}}_t + \chi(\mathbf{n} \otimes \Delta\mathbf{g}^{(k)})^s$$
$$\mathbf{R}_2^{(k)} \equiv \mathbf{n} \cdot \boldsymbol{\sigma}^{(k)} - \mathbf{t}^{(k)} \tag{34}$$

Linearizing these residuals

$$\begin{aligned}&\mathbf{R}_1^{(k)}+\partial_{\boldsymbol{\sigma}}\mathbf{R}_1^{(k)}:\delta\boldsymbol{\sigma}^{(k)}+\partial_{\mathbf{g}}\mathbf{R}_1^{(k)}\cdot\delta\mathbf{g}^{(k)}=0\\&\mathbf{R}_2^{(k)}+\partial_{\boldsymbol{\sigma}}\mathbf{R}_2^{(k)}:\delta\boldsymbol{\sigma}^{(k)}+\partial_{\mathbf{g}}\mathbf{R}_2^{(k)}\cdot\delta\mathbf{g}^{(k)}=0\end{aligned}\tag{35}$$

and substituting for the derivatives, one has

$$\begin{aligned}&\mathbf{R}_1^{(k)}+\mathbb{C}:\delta\boldsymbol{\sigma}^{(k)}+\chi(\mathbf{n}\otimes\delta\mathbf{g}^{(k)})^s=0\\&\mathbf{R}_2^{(k)}+\mathbf{n}\cdot\delta\boldsymbol{\sigma}^{(k)}-\mathbf{K}\cdot\delta\mathbf{g}^{(k)}=0\end{aligned}\tag{36}$$

Solving now Eq. (36) for stress and strain corrections, one obtains

$$\begin{aligned}\delta\mathbf{g}^{(k)}&=\left[\chi(\mathbf{n}\cdot\mathbb{D}\cdot\mathbf{n})+\mathbf{K}^{(k)}\right]^{-1}\left(\mathbf{R}_2^{(k)}-\mathbf{n}\cdot\mathbb{D}^{(k)}:\mathbf{R}_1^{(k)}\right)\\\delta\boldsymbol{\sigma}^{(k)}&=-\mathbb{D}:\left(\mathbf{R}_1^{(k)}+\chi(\mathbf{n}\otimes\delta\mathbf{g}^{(k)})^s\right)\\\delta\tilde{\boldsymbol{\varepsilon}}^{(k)}&=\mathbb{C}:\delta\mathbf{g}^{(k)}\end{aligned}\tag{37}$$

with

$$\begin{aligned}\mathbf{g}^{(k+1)}&=\mathbf{g}^{(k)}+\delta\mathbf{g}^{(k)}\\\boldsymbol{\sigma}^{(k+1)}&=\boldsymbol{\sigma}^{(k)}+\delta\boldsymbol{\sigma}^{(k)}\\\tilde{\boldsymbol{\varepsilon}}^{(k+1)}&=\tilde{\boldsymbol{\varepsilon}}^{(k)}+\delta\tilde{\boldsymbol{\varepsilon}}^{(k)}\end{aligned}\tag{38}$$

Note that the tangential operator is defined here viz Eq. (21).

## 4. Numerical study: bi-axial plane strain tests on Tournemire argillite

The numerical study presented here deals with the description of localized damage in Tournemire argillite rock subjected to plane strain biaxial compression. The focus is on examining the influence of boundary conditions, as well as the orientation of the bedding planes, on the failure mechanism and the resulting assessment of compressive strength. The study makes use of the results of triaxial tests that have been reported by Abdi et al. (2015). Those results were employed to identify the material parameters/functions that enter the formulation, as discussed in Section 2.

In general, the specification of material constants requires information on the conditions at failure as well as the deformation characteristics in samples tested at different orientation of the bedding planes and different confining pressures. Here, the results of a series of axial compression tests were employed to identify the function $\eta_f(\zeta)$ and the material parameter $C$, Eq. (6). In particular, for each specific orientation of the sample and the given confining pressure, the value of $\eta_f$ and the corresponding loading direction were determined. The results generated a set of data which was then approximated using the best-fit (i.e. least-square) procedure employing representation (4). At the same time, the hardening parameter $A$, Eq. (8), and the dilatancy constant $\alpha$, Eq. (9), were identified by examining the of deviatoric/volumetric stress characteristics for the same set of experimental data. The details on the identification procedure, are provided in the forthcoming proceedings of the ISRM Congress (Haghighat et al., 2015). Based on that study, the following parameters were selected for the anisotropic framework describing the homogeneous deformation mode, viz. Section 2.1

$$\begin{aligned}&E_n=12.5\text{ GPa},\quad E_t=21\text{ GPa},\quad G_{nt}=4.57\text{ GPa},\quad \nu_{nt}=0.16,\\&\nu_{tt}=0.08\quad \hat{\eta}_f=1.07252,\quad A_t=0.170336,\quad a_1=5.49565,\\&\alpha=0.99,\quad \xi=1.25,\quad C=10.61\text{ MPa},\quad A=0.0012\end{aligned}\tag{39}$$

where $n$, $t$ define the normal and tangential direction, respectively, in the coordinate system attached to a bedding plane. As an illustration, the spatial variation of the strength parameter $\eta_f$, Eq. (6), is depicted in Fig. 1 below.

Given the distribution of $\eta_f$ as a function of the loading angle, the corresponding values of the friction angle $\phi$ and the cohesion $c$ can be calculated from $\phi=\sin^{-1}(3\eta_f/(6+\eta_f))$ and $c=C\eta_f(3-\sin\phi)/(2\sqrt{3}\cos\phi)$, respectively. The latter values are required for identification of the critical plane framework, which is employed to define the orientation of the localization plane. The best-fit approximation, which retains the second-order terms, i.e. $\mu=\hat{\mu}(1+\Omega_{ij}n_in_j+A_1(\Omega_{ij}n_in_j)^2)$, $c=\hat{c}(1+\Omega_{ij}n_in_j+A_1(\Omega_{ij}n_in_j)^2)$ and $\mu=\tan\phi$, results in the following set of coefficients

$$\hat{\mu}=0.51063,\quad \hat{c}=5.41646,\quad \Omega_t=0.19448,\quad A_1=4.79833\tag{40}$$

The corresponding spatial variation of strength parameters is plotted in Fig. 2. It should be noted that since $C$ is defined as orientation independent, the distribution of both descriptors displays a similar bias.

For the interfacial material, once the localization occurs the parameter $\mu_f^0$, Eq. (32), is determined based on the ratio of the components of the traction vector, i.e. $\mu_f^0=-|\tau|/\sigma$. The simulations presented here were conducted assuming the following set of elastic moduli and the degradation coefficients, Eq. (32)

$$K_n=K_t=1\times10^5\text{ MPa/mm},\quad \mu_f^r=0.7\mu_f^0,\quad \omega=5.45\text{ mm}^{-1}\tag{41}$$

These values were selected on a rather intuitive basis as no explicit experimental evidence is available.

The set up for the biaxial test and the corresponding boundary conditions are shown in Fig. 3. The sample has in plane dimensions of 100 × 50 mm and out of plane thickness of 50 mm. The load was applied incrementally in two stages. The first one involved

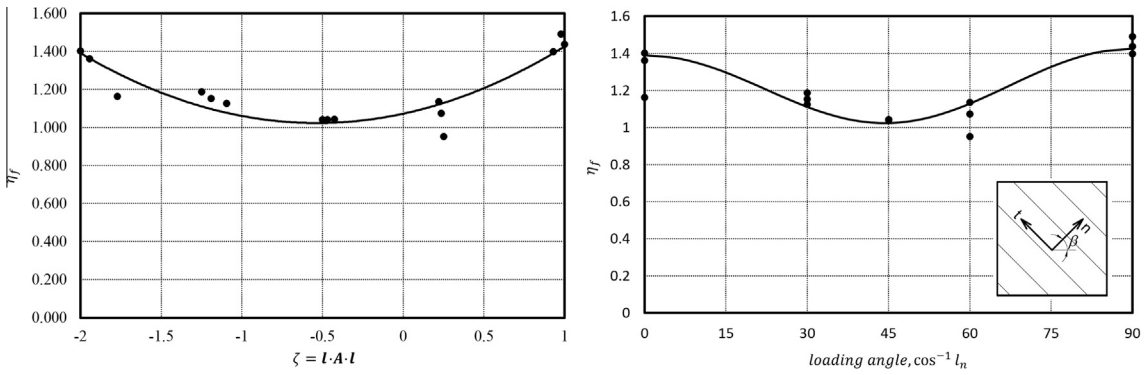


**Fig. 1.** Variation of strength parameter $\eta_f$ vs microstructure parameter $\zeta$ (left) and loading angle (right).

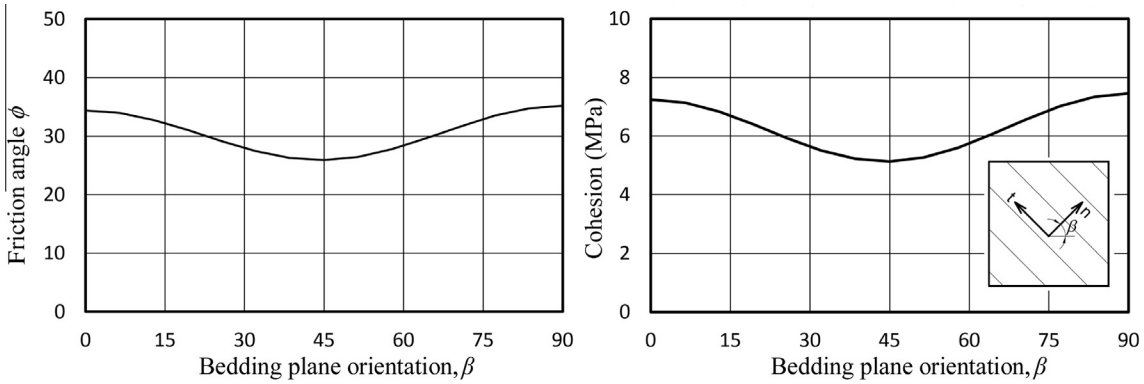


**Fig. 2.** Distribution of friction angle $\phi$ and cohesion $c$ with respect to the orientation of the bedding planes $\beta$.

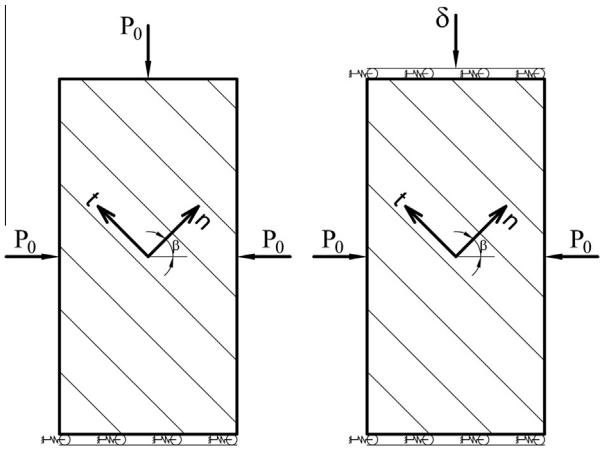


**Fig. 3.** Biaxial test configuration and boundary conditions.

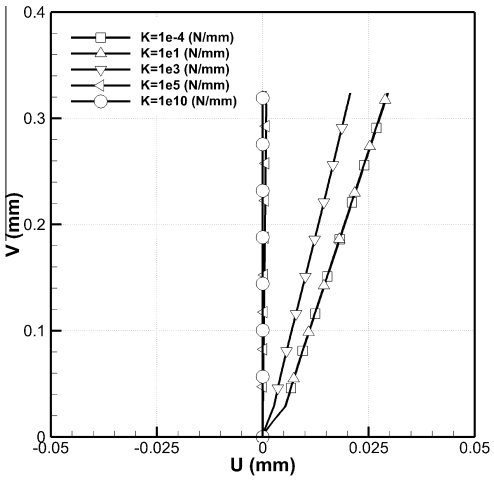


**Fig. 4.** Average horizontal sliding ($U$) at the loading platen for the case of $\beta = 45°$.

subjecting the sample to a confining pressure $P_0$. After this, the displacement field was set to zero and the vertical displacement $\delta$ was applied.

In order to simulate the actual test conditions, a simple elastic interface model was used to incorporate the effect of friction between the loading platens and the sample. Five different stiffness coefficients were employed ranging from $K = 1 \times 10^{-4}$ to $1 \times 10^{10}$ N/mm which are representative of frictionless and fully constrained (sticking friction) conditions, respectively. Fig. 4 shows the evolution of the interfacial displacement in an inclined sample, $\beta = 45°$, for different values of coefficients $K$.

Fig. 5 shows the distribution of the damage ratio $\eta/\eta_f$, which is defined according to Eqs. (8) and (6). Note that $0 \leqslant \eta/\eta_f \leqslant 1$, with $\eta/\eta_f = 1$ signifying the onset of macrocrack formation. The distribution corresponds to the instant just before the onset of localization and refers to a sample tested at $\beta = 45°$. The results shown in Fig. 5 correspond again to different frictional constraints at the end platens (viz. the coefficients $K$). It is evident from this figure that for low values of $K$, i.e. $K \leqslant 1 \times 10^1$ N/mm, the stress and deformation fields remain homogeneous. On the other hand, for $K \geqslant 1 \times 10^3$ N/mm, i.e. when the friction is more significant, the deformation is localized into a shear band/macrocrack that forms at the corners and/or at the center of the sample.

Fig. 6 shows the corresponding load–displacement characteristics, with $q$ and $V$ representing the additional vertical stress and the vertical displacement of the top platen, respectively. As can be seen here, the value of the coefficient $K$ significantly affects the ultimate (peak) load. This implies that the friction between loading platens and the sample plays an important role in the assessment of both the load capacity and the actual failure mode of the sample.

Fig. 7 shows the evolution of the damage ratio $\eta/\eta_f$ just before the onset of localization for tests conducted at different orientations of the bedding planes. The results correspond to $K \geqslant 1 \times 10^5$ N/mm. It is evident here that in case of horizontal and vertical bedding planes, the failure mode is largely diffused while for the inclined samples, there is an indication of a shear band/macrocrack formation. The actual failure mechanism, as obtained from numerical simulations, is depicted in Fig. 8 for various bedding planes orientations.

The last study conducted here deals with the issue of the mesh dependency of the solution based on the approach followed in this work. The key results are shown in Figs. 9 and 10. The simulations involved three different discretizations. The basic mesh, i.e. mesh 1, is identical to the one employed in all simulations presented earlier. Mesh 2 is a refined structured mesh while mesh 3 is an unstructured mesh that is oriented along the direction of the shear band corresponding to the localization pattern predicted from the previous meshes. The load-displacement cures are provided in Fig. 9, whereas Fig. 10 shows the deformed shape with the scale factor of 10. It is quite evident here that the solution is mesh-independent, i.e. the ultimate load as well as deformation pattern are virtually the same.

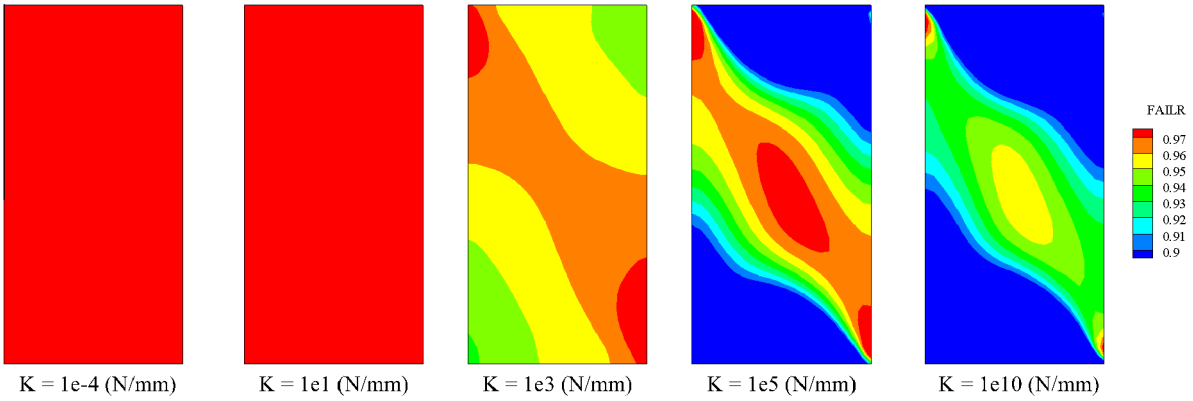


**Fig. 5.** Damage ratio $\eta/\eta_f$ for different values of friction at the end platens; $\beta = 45°$. (For interpretation to colours in this figure, the reader is referred to the web version of this paper.)

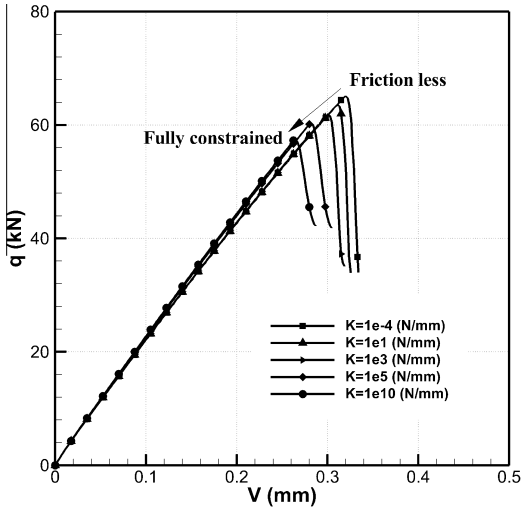


**Fig. 6.** Load displacement curves for different values of friction at the end platens; $\beta = 45°$.

## 5. Final remarks

In this study, the problem of the description of deformation and progressive damage in anisotropic rock formations was examined. The deformation prior to failure was described using an elasto-plastic formulation incorporating the microstructure tensor approach. The predictive abilities of this framework have been studied before (e.g. Pietruszczak et al. (2002)). Here, the primary focus was on modeling of the failure mode associated with strain localization. The onset of macrocracking was defined by employing a simple stress criterion formulated within the context of a deviatoric hardening. The orientation of the localization plane was then established based on the critical plane approach by extracting the corresponding strength parameters from the elasto-plastic model. The constitutive law with embedded discontinuity was used to describe the post failure response associated with localized deformation. The discrete propagation of damage was monitored trough the level-set method. The closest-point projection integration scheme was derived for both the anisotropic deviatoric hardening model and the constitutive law with embedded discontinuity.

The mechanical characteristics of Tournemire shale were examined and the effect of boundary condition on the shear band formation was investigated for a series of biaxial plane strain compression tests. It was shown that in the case of a frictionless interface between loading platens and the sample, the deformation field remains homogeneous and the failure mode is diffused. With a presence of friction, however, the stress state is significantly perturbed which results in formation of a shear band/macrocrack. In this case, the ultimate strength of the sample is noticeably less than the one attained under frictionless conditions. A series of simulations for samples with different orientations of bedding planes was also conducted. It was shown that in samples with horizontal and vertical bedding planes, the failure mode is diffused for both frictionless and fully constrained cases; however the peak strength is still noticeably different for both these cases.

Finally, the mesh-dependency of the solution was examined using three different discretizations. Two structured meshes of different size and one mesh oriented along the direction of shear band

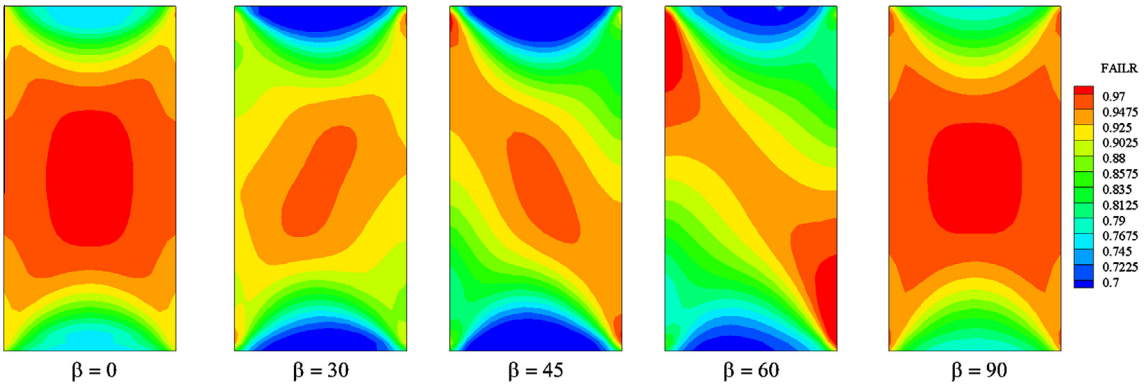


**Fig. 7.** Damage ratio $\eta/\eta_f$ at the crack initiation for different orientations of bedding planes $\beta$; $K \geqslant 1 \times 10^5\ N/mm^2$. (For interpretation to colors in this figure, the reader is referred to the web version of this paper.)

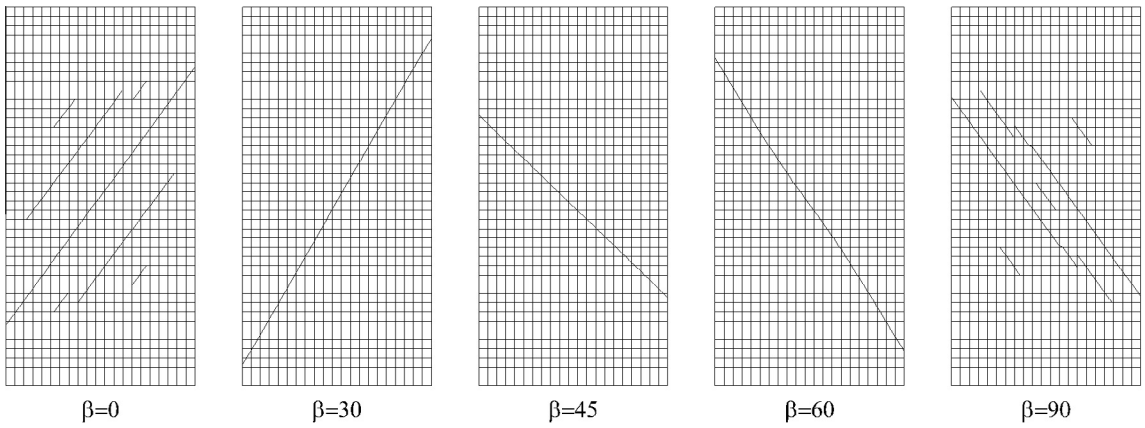


**Fig. 8.** The predicted failure pattern in samples tested at different orientation of bedding planes $\beta$.

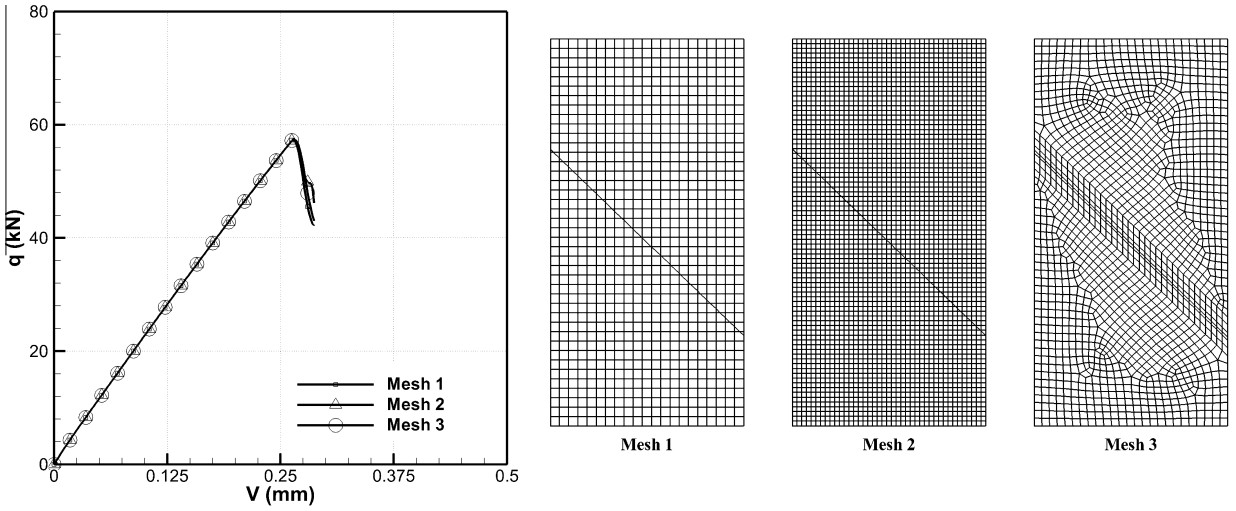


**Fig. 9.** Load displacement response for various FE meshes; the case of $\beta = 45^{\circ}$ with $K \geqslant 1 \times 10^5\ N/mm^2$.

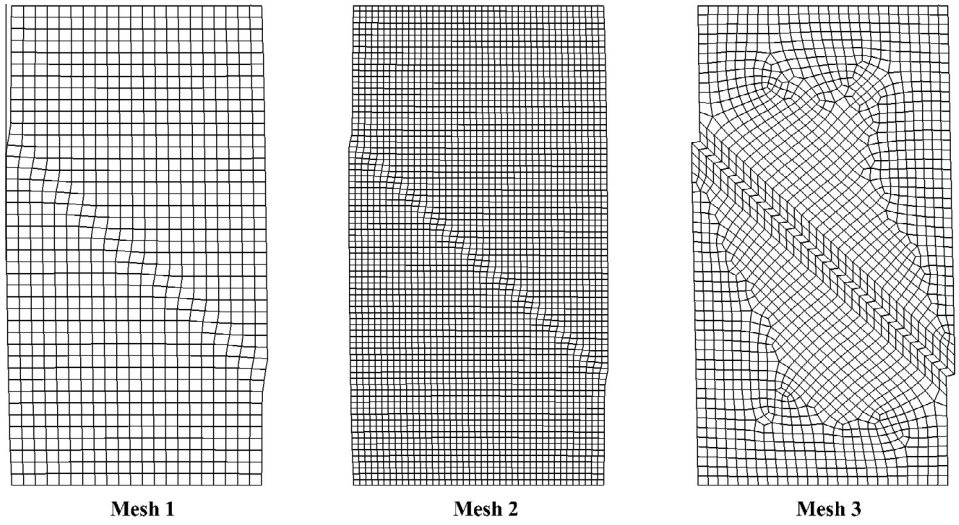


**Fig. 10.** Deformed mesh plots for various discretizations; scale factor of 10.

were employed. It was concluded that by invoking the constitutive law with embedded discontinuity, which incorporates a characteristic dimension, the solution is virtually mesh independent.

## References


Abdi, H., Labrie, D., Ngyuen, T.S., Barnichon, J.D., Su, G., Evgin, E., Simon, R., Fall, M., 2015. Laboratory investigation on the mechanical behaviour of Tournemire agrillite. Can. Geotech. J. 52, 268–282.

Amadei, B., 1983. Rock Anisotropy and the Theory of Stress Measurements. Springer-Verlag, Berlin.

Bažant, Z.P., Cedolin, L., 1979. Blunt crack band propagation in finite element analysis. Int. J. Eng. Mech. ASCE 105, 297–315.

Belytschko, T., Black, T., 1999. Elastic crack growth in finite elements with minimal remeshing. Int. J. Numer. Methods Eng. 45, 601–620.

Belytschko, T., Gu, L., Lu, Y.Y., 1994. Fracture and crack growth by element free Galerkin methods. Model. Simul. Mater. Sci. Eng. 2, 519–534.

Boehler, J.P., Sawczuk, A., 1977. On yielding of oriented solids. Acta Mech. 27, 185–204.

Chessa, J., Belytschko, T., 2003. An enriched finite element method and level sets for axisymmetric two-phase flow with surface tension. Int. J. Numer. Methods Eng. 58, 2041–2064.

Duveau, G., Henry, J.P., 1998. Assessment of some failure criteria for strongly anisotropic geomaterials. Mech. Cohesive-frictional Mater. 3, 1–26.

Fish, J., Belytschko, T., 1988. Elements with embedded localization zones for large deformation problems. Comput. Struct. 30, 247–256.

Haghighat, E., Pietruszczak, S., 2015. On modeling of discrete propagation of localized damage in cohesive-frictional materials. Int. J. Numer. Anal. Methods Geomech. http://dx.doi.org/10.1002/nag.2368.

Haghighat, E., Pietruszczak, S., Su, G., Nguyen, T.S., 2015. Numerical investigation of the mechanical behaviour of Tournemire argillite. In: Proceedings ISRM. http://dx.doi.org/10.1007/BF01180085.

Hill, R., 1950. The Mathematical Theory of Plasticity, vol. 328. Oxford University Press.

Ingraffea, A.R., 1977. Nodal grafting for crack propagation studies. Int. J. Numer. Methods Eng. 11, 1185–1187.

Kwasniewski, M.A., 1993. Mechanical Behavior of Anisotropic Rocks. Comprehensive Rock Engineering. Pergamon Press, Oxford, pp. 285–312.

Lade, P.V., 2007. Modeling failure in cross-anisotropic frictional materials. Int. J. Solids Struct. 44, 5146–5162.

Liu, W.K., Jun, S., Zhang, Y.F., 1995. Reproducing kernel particle methods. Int. J. Numer. Methods Fluids 20, 1081–1106.

Melenk, J.M., Babuška, I., 1996. The partition of unity finite element method: basic theory and applications. Comput. Methods Appl. Mech. Eng. 139, 289–314.

Moës, N., Dolbow, J., Belytschko, T., 1999. A finite element method for crack growth without remeshing. Int. J. Numer. Methods Eng. 46, 131–150.

Nayak, G.C., Zienkiewicz, O.C., 1972. Elasto-plastic stress analysis. A generalization for various constitutive relations including strain softening. Int. J. Numer. Methods Eng. 5, 113–135.

Ngo, D., Scordelis, A.C., 1967. Finite element analysis of reinforced concrete beams. ACI Struct. J. Proc. 64, 152–163.

Nova, R., 1980. The failure of transversely isotropic rocks in triaxial compression. Int. J. Rock Mech. Min. Sci. Geomech. Abstr. 17, 325–332.

Pariseau, W.G., 1968. Plasticity theory for anisotropic rocks and soil. In: Proceedings 10th Inten. Symp. Rock Mech., Amer. Rock. Mech. Assoc.

Pietruszczak, S., 1999. On homogeneous and localized deformation in water-infiltrated soils. Int. J. Damage Mech. 8, 233–253.

Pietruszczak, S., Lydzba, D., Shao, J.F., 2002. Modelling of inherent anisotropy in sedimentary rocks. Int. J. Solids Struct. 39, 637–648.

Pietruszczak, S., Mroz, Z., 1981. Finite element analysis of deformation of strain-softening materials. Int. J. Numer. Methods Eng. 17, 327–334.

Pietruszczak, S., Mroz, Z., 2001. On failure criteria for anisotropic cohesive-frictional materials. Int. J. Numer. Anal. Methods Geomech. 25, 509–524.

Rabczuk, T., Belytschko, T., 2007. A three-dimensional large deformation meshfree method for arbitrary evolving cracks. Comput. Methods Appl. Mech. Eng. 196, 2777–2799.

Rashid, Y.R., 1968. Ultimate strength analysis of prestressed concrete pressure vessels. Nucl. Eng. Des. 7, 334–344.

Rudnicki, J.W., Rice, J.R., 1975. Conditions for the localization of deformation in pressure-sensitive dilatant materials. J. Mech. Phys. Solids 23, 371–394.

Simo, J., 1998. Computational Inelasticity. Springer-Verlag, Berlin.

Simo, J.C., Oliver, J., Armero, F., 1993. An analysis of strong discontinuities induced by strain-softening in rate-independent inelastic solids. Comput. Mech. 12, 277–296.

Sukumar, N., Chopp, D.L., Moës, N., Belytschko, T., 2001. Modeling holes and inclusions by level sets in the extended finite-element method. Comput. Methods Appl. Mech. Eng. 190, 6183–6200.

Sukumar, N., Moës, N., Moran, B., Belytschko, T., 2000. Extended finite element method for three-dimensional crack modelling. Int. J. Numer. Methods Eng. 48, 1549–1570.